



Fatty Acid Synthesis Knockdown Promotes Biofilm Wrinkling and Inhibits Sporulation in *Bacillus subtilis*

Heidi A. Arjes, ^a Haiwen Gui, ^a Rachel Porter, ^b Esha Atolia, ^a Dason M. Peters, ^{c,d,e,f} Carol Gross, ^{g,h} Daniel B. Kearns, ⁱ Kerwyn Casey Huang ^{a,j,k}

- ^aDepartment of Bioengineering, Stanford University School of Medicine, Stanford, California, USA
- ^bDepartment of Molecular and Cellular Physiology, Stanford University School of Medicine, Stanford, California, USA
- cPharmaceutical Sciences Division, School of Pharmacy, University of Wisconsin—Madison, Madison, Wisconsin, USA
- dGreat Lakes Bioenergy Research Center, Wisconsin Energy Institute, University of Wisconsin—Madison, Madison, Wisconsin, USA
- eDepartment of Bacteriology, University of Wisconsin—Madison, Madison, Wisconsin, USA
- Department of Medical Microbiology and Immunology, University of Wisconsin—Madison, Madison, Wisconsin, USA
- ⁹Department of Microbiology and Immunology, University of California San Francisco, San Francisco, California, USA
- ^hDepartment of Cell and Tissue Biology, University of California San Francisco, San Francisco, California, USA
- Department of Biology, Indiana University, Bloomington, Indiana, USA
- Department of Microbiology and Immunology, Stanford University School of Medicine, Stanford, California, USA
- kChan Zuckerberg Biohub, San Francisco, California, USA

ABSTRACT Many bacterial species typically live in complex three-dimensional biofilms, yet much remains unknown about differences in essential processes between nonbiofilm and biofilm lifestyles. Here, we created a CRISPR interference (CRISPRi) library of knockdown strains covering all known essential genes in the biofilm-forming Bacillus subtilis strain NCIB 3610 and investigated growth, biofilm colony wrinkling, and sporulation phenotypes of the knockdown library. First, we showed that gene essentiality is largely conserved between liquid and surface growth and between two media. Second, we quantified biofilm colony wrinkling using a custom image analysis algorithm and found that fatty acid synthesis and DNA gyrase knockdown strains exhibited increased wrinkling independent of biofilm matrix gene expression. Third, we designed a high-throughput screen to quantify sporulation efficiency after essential gene knockdown; we found that partial knockdowns of essential genes remained competent for sporulation in a sporulation-inducing medium, but knockdown of essential genes involved in fatty acid synthesis exhibited reduced sporulation efficiency in LB, a medium with generally lower levels of sporulation. We conclude that a subset of essential genes are particularly important for biofilm structure and sporulation/germination and suggest a previously unappreciated and multifaceted role for fatty acid synthesis in bacterial lifestyles and developmental processes.

IMPORTANCE For many bacteria, life typically involves growth in dense, three-dimensional communities called biofilms that contain cells with differentiated roles held together by extracellular matrix. To examine how essential gene function varies between vegetative growth and the developmental states of biofilm formation and sporulation, we created and screened a comprehensive library of strains using CRISPRi to knockdown expression of each essential gene in the biofilm-capable *Bacillus subtilis* strain 3610. High-throughput assays and computational algorithms identified a subset of essential genes involved in biofilm wrinkling and sporulation and indicated that fatty acid synthesis plays important and multifaceted roles in bacterial development.

KEYWORDS CRISPR interference, biofilms, spatial organization, essential genes, high-throughput screening, sporulation

Editor Matthew Parsek, University of Washington

Copyright © 2022 Arjes et al. This is an openaccess article distributed under the terms of the Creative Commons Attribution 4.0

Address correspondence to Kerwyn Casey Huang, kchuang@stanford.edu.

The authors declare no conflict of interest.

Received 30 May 2022 Accepted 5 August 2022

10.1128/mbio.01388-22

any bacterial species grow in dense, three-dimensional communities held together by extracellular matrix (1). These communities, often called biofilms, represent a form of multicellularity as they typically contain cells with differentiated roles (2, 3). Although biofilm development has recently gained attention as an evolutionary strategy among microbes (3), many aspects of how biofilm development impacts bacterial fitness remain mysterious. The Gram-positive bacterium *Bacillus subtilis* has the ability to transition from a motile to a sessile state and has served as a model organism to study both planktonic and biofilm lifestyles (4). Moreover, when *B. subtilis* encounters stressful environments, such as nutrient limitation, it can differentiate into a spore that can withstand harsh conditions until the environment is favorable for growth (5).

While *B. subtilis* has been cultivated in laboratories for over a century, most studies have purposefully focused on laboratory strains that are deficient in biofilm formation, and it remains unclear how findings based on these strains translate to wild strains that can form biofilms. For instance, sporulation has been studied extensively, but almost exclusively in laboratory strains using screens to identify nonessential gene disruptions that affect sporulation. Recently, two genome-scale screens of nonessential genes of *B. subtilis* laboratory strain 168 revealed an additional 73 (6) and 24 genes (7) linked to sporulation in addition to the >100 genes that had already been identified, suggesting the potential for further discovery involving this developmental process. Moreover, the role of essential genes in sporulation remains uncharacterized.

B. subtilis can live as planktonic cultures or as a biofilm that contains cells in many differentiated states, including both motile and sessile cells (8–11). Early in biofilm development, cells grow by consuming nutrients from an agar (colony biofilm) or a liquid (pellicle) surface (4). As development progresses, *B. subtilis* colony biofilms adopt a characteristic wrinkling pattern involving buckling of the multilayered structure perpendicular to the surface, correlated with areas in which localized cell death had previous occurred (12). Wrinkle formation is dependent on extracellular matrix production (13) and adhesion to the substratum (12, 14), and wrinkles can transport liquid through the biofilm (15). While some of the genetic regulation underlying wrinkling has been elucidated, the roles of essential genes in biofilm wrinkling and whether essential processes mechanistically connect wrinkling to other aspects of development such as sporulation are largely unknown.

In a previous study, we systematically explored the function of essential genes in *B. subtilis* laboratory strain 168 using a CRISPR interference (CRISPRi) gene knockdown library. We showed that dCas9 (nuclease-deactivated Cas9) induction could be used to control expression of RFP in a titratable manner, resulting in ~30% expression of the target gene at basal levels of dCas9 induction and gradual titration down to essentially 0% expression with full induction, with repression relatively homogenous across a population of cells grown in liquid culture (16). In a separate study, we demonstrated that CRISPRi can effectively knockdown genes in three-dimensional colonies of a green fluorescent protein (GFP)-labeled version of the biofilm-forming strain 3610 (17), indicating that CRISPRi is a useful tool for probing essential gene knockdowns both in liquid and on an agar surface. These genetic tools provide the opportunity to evaluate the role of essential genes in bacterial developmental processes such as nonbiofilm and multicellular biofilm colony growth, biofilm wrinkling, and sporulation.

Here, we study a comprehensive library of strains capable of depleting essential gene products in *B. subtilis* strain 3610. We demonstrate that knockdown of gene expression is effective in biofilms over 48 h, a common time scale of *B. subtilis* biofilm experiments. We find that the subsets of genes essential for growth largely overlap between liquid and colony growth and between two media. We developed high-throughput assays to quantify biofilm wrinkling and sporulation, which revealed that knockdown of fatty acid synthesis genes or gyrase enhances biofilm wrinkling uncorrelated with changes to matrix gene expression and that knockdown of fatty acid synthesis reduces sporulation efficiency. Together, these findings highlight the utility of systems-scale approaches to elucidate the functions of essential genes in planktonic and community behaviors.

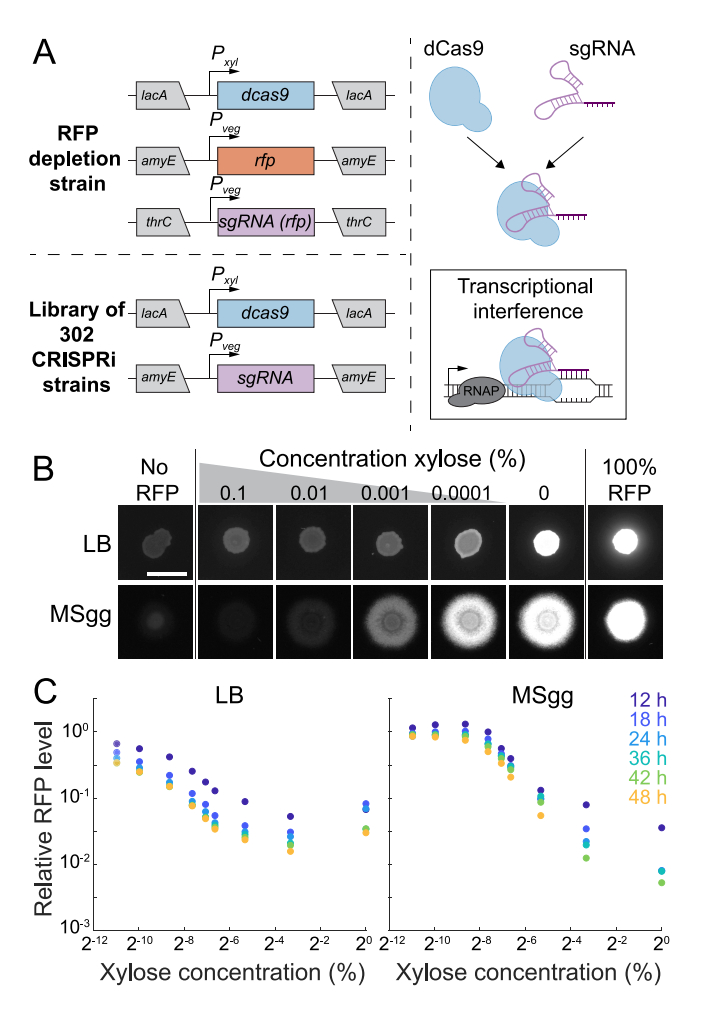


FIG 1 CRISPRi effectively inhibits gene expression during colony growth on LB and MSgg agar. (A) In this study, a CRISPRi library was created to individually inhibit the expression of each essential gene and select nonessential genes. (Left) The nuclease-deactivated Cas9 (dcas9) gene was inserted under a xylose-inducible promoter (P_{xy}) at the lacA locus. For the control RFP depletion strain (top), the rfp gene was inserted under the control of a vegetative promoter (P_{veg}) at the amyE locus and a P_{veg} -rfp-targeting sgRNA construct was inserted at the thrC locus. For the library of 302 strains, a P_{veg} -gene targeting sgRNA construct was inserted at the amyE locus. (Right) dCas9 binds to the sgRNA and inhibits transcription. (B) CRISPRi effectively inhibits expression in colonies grown on LB or MSgg and is titratable. Colonies were spotted onto plates with various concentrations of xylose at t=0 h, and RFP fluorescence at 24 h is shown. All images were contrast adjusted identically. Scale bar, 5 mm. (C) CRISPRi knockdown remains effective for at least 48 h in colonies on LB and MSgg and has greater dynamic range on MSgg. RFP fluorescence was quantified from colonies grown with various concentrations of xylose for 12, 18, 24, 36, 42, and 48 h. RFP levels decreased over time and with xylose concentration.

RESULTS

CRISPRi is an efficient mechanism for gene repression in a biofilm. To investigate the role of essential genes in colony biofilm formation, we first tested whether CRISPRi repression persisted through 48 h of colony growth on agar surfaces, a typical interval for biofilm development. We utilized a *B. subtilis* 3610 strain expressing red fluorescent protein (RFP) along with constitutive expression of a single guide RNA (sgRNA) targeting the *rfp* gene and xylose-inducible expression of dCas9 (Fig. 1A; see Table S1 in the supplemental material) (17). We grew this RFP depletion strain on agar plates with the undefined rich medium LB and on plates with the defined, biofilm-promoting medium MSgg, with various concentrations of xylose to cover a range of induction from basal (no xylose) to full knockdown (1% xylose). Repression of *rfp* was generally titratable with increasing concentrations of xylose, with a relatively uniform RFP signal across the colony at each xylose concentration (Fig. 1B). In colonies on LB, RFP intensity decreased by \sim 20-fold with full knockdown (Fig. 1C; Fig. S1). The dynamic range was even greater in biofilm colonies grown on MSgg, with an \sim 100-fold intensity

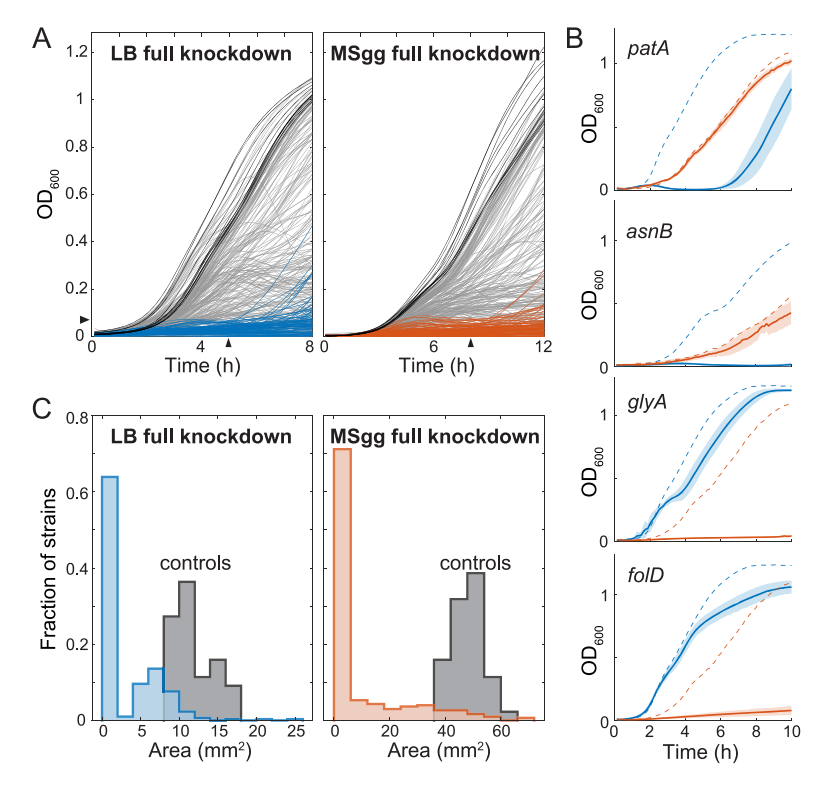


FIG 2 Systematic quantification reveals essential gene knockdowns with medium-specific growth phenotypes. (A) Full knockdown of many essential genes in liquid media (left, LB+1% xylose; right, MSgg+1% xylose) led to growth impairment. Black lines show the parent control, and blue (left) or orange (right) lines show strain 3610 knockdown strains with poor growth ($OD_{600} < 0.075$) at 5 h (left) or 8 h (right). (B) Four gene knockdowns exhibited dramatically different growth patterns in LB+1% xylose and MSgg+1% xylose. patA and asnB full knockdowns grew better in MSgg than in LB. glyA and folD full knockdowns grew better in LB than in MSgg. Dashed lines show the average of the parent control in each medium: the asnB full knockdown and the corresponding control were grown at 30°C, while all other cultures were grown at 37°C. Blue and orange lines represent growth in LB+1% xylose and MSgg+1% xylose, respectively. Solid lines are the average growth curve over n = 6 biological replicates, and shading represents 1 standard deviation. (C) Full knockdown of many genes resulted in growth impairment on solid medium. Colony sizes at 24 h are plotted. Parent controls (n = 44) are shown in gray.

reduction (Fig. 1C). Thus, we conclude that CRISPRi is a useful tool for inhibiting the expression of essential genes in *B. subtilis* 3610 on surfaces for both LB and MSgg media.

Gene essentiality is largely conserved between liquid and colony growth. A previous study determined gene essentiality in *B. subtilis* strain 168 based on the ability to delete the gene of interest during growth in LB (6). Strain 168 has genetic differences relative to strain 3610 in genes important for biofilm formation and other social behaviors, such as swarming (18). Nonetheless, we found that the 252 genes described as essential in strain 168 were 100% conserved at the protein sequence level in 3610 (Materials and Methods). Thus, we constructed a library of 302 CRISPRi gene knockdowns in *B. subtilis* strain 3610 (Materials and Methods) (Table S1) (16), which includes the 252 genes identified to be essential in *B. subtilis* 168, 47 conditionally essential and nonessential genes, and 3 controls that do not express an sgRNA. All strains grew as colonies on both LB and MSgg in the absence of inducer (Fig. S2A), demonstrating that basal knockdown of any of these genes remained viable.

We next determined the extent to which the genes targeted in our library are necessary for growth under our experimental conditions in or on LB and MSgg media (Fig. 2A). In liquid LB plus 1% xylose (LB+xylose) to induce dCas9 and fully knock down the gene target, 111 full knockdowns in strain 3610 did not grow substantially (characterized as an optical density at 600 nm [OD $_{600}$] of <0.075 at 5 h) (Fig. 2A; Table S2). In liquid MSgg+1% xylose, 129 full knockdowns in strain 3610 did not grow (characterized as OD $_{600}$ of <0.075 at 8 h) (Fig. 2A; Table S2), of which 102 also failed to grow in LB+1% xylose (Table S2).

Under these growth conditions and cutoffs, we identified 27 genes that were potentially required for growth in MSgg but not in LB and 9 genes that were potentially required in LB but not in MSgg. Closer inspection revealed that many of these hits were false positives, as growth of the full knockdown was slightly above the cutoff in one medium; only 4 of the 36 were true positives (Fig. S2B). Full knockdown of *patA* and *asnB*, which are involved in lysine and asparagine synthesis, respectively, inhibited growth in LB+1% xylose but not MSgg+1% xylose (Fig. 2B; Fig. S2B), consistent with the medium dependence of the fitness of *patA* and *asnB* knockdowns when grown on plates in competition with wild-type cells (17). Full knockdown of *glyA* and *folD*, which are involved in glycine and folate synthesis, respectively, inhibited growth in MSgg+xylose but not LB+xylose (Fig. 2B, Fig. S2B); *glyA* displayed a medium-dependent competitive fitness when grown on plates with wild-type cells and fitness increased when glycine was added to MSgg+1% xylose (17), confirming that *glyA* is conditionally essential and *glyA* knockdowns require glycine for growth. It remains to be determined whether the *folD* medium-specific phenotype is generally due to medium composition or another factor(s).

Since mutant phenotypes can vary between growth in liquid and on solid surfaces (17), we next investigated full knockdown phenotypes on LB and MSgg agar plates. 193 and 195 strains exhibited severe growth defects when grown on LB+1% xylose and MSgg+1% xylose, respectively, with an overlap of 167 strains between these two subsets (Fig. 2C; Table S3). We defined "severe growth defects" as either the absence of growth, generation of suppressors identified as petal-like projections from the original inoculation region (Fig. 2C [e.g., accD]), or failure to grow beyond the original inoculation region after 24 h (Fig. S2A and Table S3).

In sum, the majority of the genes targeted in the library that were previously identified as essential in *B. subtilis* strain 168 through deletion studies remained important for growth in strain 3610 in liquid and on solid media.

Enhancement of colony biofilm wrinkling in fatty acid and gyrase knockdowns is not correlated with expression of matrix-production genes. The defined, biofilm-promoting medium MSgg promoted a broader range of colony size phenotypes than LB (Fig. 3A; Fig. S2A), similar to our previous study (17). Since growth on MSgg agar promotes biofilm development and wrinkle formation in wild-type *B. subtilis* strain 3610, we used this medium to screen for mutants with aberrant wrinkling patterns. On MSgg, the CRISPRi library exhibited a broad variety of wrinkling patterns across strains, ranging from flat to more wrinkled than wild type. To quantify wrinkling patterns, we developed an image analysis algorithm and an associated wrinkling metric. Wrinkling intensity was quantified as the number of pixels above a threshold after images were background subtracted, contrast adjusted, and binarized (Materials and Methods) (Fig. 3B; Fig. S3B). We used this metric to quantify wrinkling across the library for basal knockdown strains and identified several strains with lower and higher wrinkling propensity than the wild type (Fig. 3C; Fig. S3A and Table S4).

We validated our wrinkling metric by manually curating the positive hits. Nine strains were identified as having high wrinkling intensity per unit area (Fig. S3A). Of these, two (murA and frr) turned out to be false positives that were misidentified due to the non-wildtype coloring of the colonies (Fig. S3A). The remaining seven strains clearly exhibited high wrinkling (Fig. 3C; Table S4); of these, the genes accB, accC, accD, and fabD have defined roles in fatty acid synthesis, and the yqhY mutant has recently been connected to fatty acid synthesis (19), although its exact role within the pathway remains unclear. Strains with knockdowns of gyrA and gyrB, encoding subunits A and B of DNA gyrase, respectively, also displayed enhanced wrinkling (Fig. 3C). Gyrase relaxes positive supercoils and introduces negative supercoils in DNA and is important for controlling DNA replication initiation and resolving head-on DNA replication-transcription conflicts (20-22); thus, their knockdown likely results in global gene expression changes. We verified the enhanced wrinkling of these seven strains (Fig. S3C) and chose four for further analysis. Since overexpression of matrix components is known to increase wrinkling (23), we quantified the expression of matrix genes in colony biofilms using promoter fusions to the eps operon and tapA (yaxM). Interestingly, expression of reporter genes under the expression of the eps or tapA promoters was significantly reduced relative to the parent control in all gene depletion strains

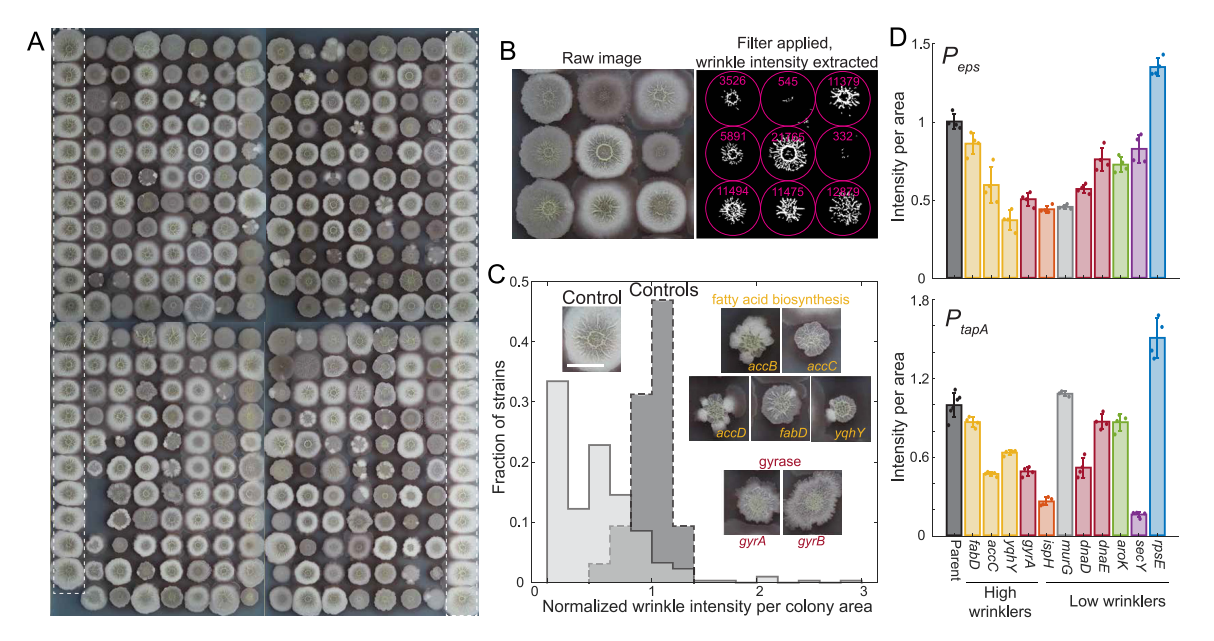


FIG 3 Knockdown of fatty acid synthesis leads to increased wrinkling density. (A) Our library of 302 gene knockdowns in strain 3610 covered a variety of wrinkling phenotypes when grown on MSgg agar plates for 48 h. Wild-type controls are outlined in white dotted rectangles. The distance between the centers of adjacent colonies is 9 mm. (B) The image analysis platform (Materials and Methods) automatically quantified the degree of wrinkling for each strain. The total wrinkling level (white pixels postprocessing) within the colony boundary (pink circles) was extracted for each colony. (C) Many strains exhibited significantly lower wrinkling than parent controls, while fatty acid and gyrase knockdowns exhibited higher wrinkling density (wrinkling intensity normalized to colony area). The dark gray dashed histogram represents the parent control, and the light gray histogram represents the 302 strains from the gene knockdown library. Insets show representative images of strains with higher wrinkling density. Scale bar, 5 mm. (D) Matrix gene (eps and tapA) expression is uncorrelated with wrinkling density. Reporter levels are shown, normalized so that the average parent control was 1. All P_{eps} -mNeongreen gene knockdown strains were significantly different from the parent control (P < 0.016). Fatty acid mutants are in yellow, DNA replication-related mutants are in red, ribosome-related mutants are in blue, cell-wall-related mutants are in gray, biosynthesis mutants are in green, and a secretion mutant is in purple. For P_{topA} -mNeongreen, all gene knockdowns except for murG were statistically significant (P < 0.045).

that displayed high wrinkling (Fig. 3D; Fig. S3D). Thus, increased matrix gene expression was not correlated with the increased wrinkling of these strains.

In addition, several colonies were much less wrinkled than the controls. We manually identified 38 relatively flat colonies by eye; of these, 37 were also identified by our computational analysis with a cutoff of 0.2 when normalized to internal controls (Materials and Methods). Strains targeting ribosomal proteins were enriched among the 38 low wrinklers compared to the entire library (DAVID analysis, $P = 8 \times 10^{-5}$). We verified the wrinkling pattern of 13 selected low wrinklers (Fig. S3A and C) and chose 11 candidates to explore further (Table S4). Since reduced matrix expression can lead to flat colonies, we tested matrix expression levels in the flat mutants using the reporter genes under the expression of the eps or tapA promoters (Fig. 3D; Fig. S3D). Knockdown of aroK resulted in significantly reduced expression of eps and tapA (Fig. 3D; Fig. S3D). In contrast, rpsE knockdown colonies displayed higher expression of both matrix genes, even though these colonies did not wrinkle (Fig. 3D; Fig. S3D), again demonstrating that wrinkling can be decoupled from matrix gene expression in some cases. The remaining candidates displayed a range of expression patterns, most with reduced expression of eps and tapA (Fig. 3D; Fig. S3D). Thus, our data suggest that flat colony phenotypes may be partly due to reduced matrix levels but that other factors can also play a role.

A high-throughput assay of sporulation efficiency based on optical density. *B. subtilis* laboratory strains have long been used as a model to study sporulation, and \sim 150 non-essential genes required for efficient sporulation and germination have been identified through a variety of screening strategies (24–31). Some of these genes are expressed during sporulation under the control of a sporulation sigma factor (32–36), while others cause a reduction in sporulation efficiency when deleted. Many of these screens relied on transposon insertion screening (7, 37) or on gene knockout libraries (6) and hence focused on only non-essential genes; thus, the role of essential genes in sporulation remains unknown.

Some genes involved in sporulation were identified based on the inability of nonsporulating mutants to produce a pigmented protein that alters the color of spore-containing colonies (6). However, while strain 168 colonies become more translucent when sporulation is blocked, we found that colonies of known sporulation mutants of strain 3610 remained opaque (Fig. S4A), rendering color-based screening ineffective. Thus, to investigate the role of essential genes in sporulation of strain 3610, we devised a straightforward, optical density-based, high-throughput screening strategy. We grew strains for 24 h and transferred the cultures to 80°C for 30 min to heat kill all vegetative cells (Fig. 4A). After the heat kill, we diluted cultures into fresh medium so that any viable spores would germinate and grow (Fig. 4A). Notably, our screening strategy by itself does not discriminate between sporulation and germination defects, as both defects would manifest as a growth delay in our assay, although germination defects can be inferred in cases where the sporulation efficiency as measured by CFU counts is near that of wild type.

To validate our assay, we grew known 168 and 3610 sporulation mutants in a sporulationinducing medium (Difco sporulation medium [DSM]) for 24 h and monitored OD₆₀₀. Growth curves were reproducible and distinct for the sporulation mutants of each strain relative to the wild type, and strain 3610 reached a higher OD₆₀₀ than strain 168, likely due to increased oxygen diffusion mediated by surfactin (Fig. 4B, left) (38). Following heat kill, wild-type cultures displayed robust growth, indicating the presence of spores as expected (Fig. 4B, right). Many sporulation mutants ($\Delta spo0A$, $\Delta sigF$, $\Delta sigF$, $\Delta sigG$, and $\Delta sigK$) displayed no growth after heat killing, demonstrating the complete absence of spores capable of germination (Fig. 4B, right). Intriguingly, heat killing of a $\Delta yafL$ mutant that is known to undergo reduced sporulation (7) exhibited a substantial increase in lag time after heat killing relative to the wild type in the strain 168 background, but its lag in the strain 3610 background was similar to that of the wild type, suggesting that this mutant phenotype may be dependent on strain background (Fig. 4B, right). Regardless, these data indicate that our assay successfully identifies mutants fully blocked for sporulation and/or germination and can identify mutants with partially reduced sporulation. Note that this screening method will not identify mutations that are involved in sporulation but do not reduce sporulation efficiency.

We noticed that strain 168 exhibited a \sim 1-h delay in outgrowth compared to strain 3610 (Fig. 4B, right). After 24 h of growth in DSM, the total number of CFU after heat-killing (Fig. 4C) and the sporulation efficiency (ratio of CFU post-heat-kill spores to pre-heat-kill spores and viable cells) (Fig. 4D) were reduced 2- to 2.5-fold in strain 168 compared to strain 3610. Thus, the reduced number of germination-capable spores produced by strain 168 relative to strain 3610 underlies the increased time until growth was observed in strain 168.

We tested whether outgrowth dynamics after heat killing could serve as a quantitative proxy for spore counts by measuring the lag time (defined as the time to reach an OD₆₀₀ of 0.2) for 10-fold serial dilutions of strain 168 or strain 3610 after 24 h of growth in DSM and heat killing. Undiluted inocula exhibited the shortest lag times, and the lag time was highly correlated with spore count (Fig. 4E), with an additional delay of \sim 1 h for each 10-fold dilution (Fig. 54B), consistent with a doubling time of \sim 20 min. Based on 1 spore being present within the 1- μ L inoculum, our assay has a limit of detection of \sim 10³ CFU/mL of the original culture (Fig. 4E); this limit could presumably be decreased further by increasing the inoculum size. Taken together, these data demonstrate that lowering the number of spores in the inoculum results in predictable delays in outgrowth and that our assay enables high-throughput quantification of sporulation/germination efficiency.

All essential gene knockdown strains are competent for sporulation and germination under basal CRISPRi induction in a sporulation medium. To probe whether any strains in our CRISPRi library in the strain 3610 background had a reduced ability to sporulate or germinate, we applied our OD-based sporulation assay under basal knockdown conditions after growth in DSM for 24 h. We selected basal knockdown conditions as full knockdown promotes the emergence of suppressors in strains that are defective for growth (16). During growth in DSM, even though known sporulation mutants displayed distinct growth dynamics (Fig. 4B, right), there was too much variability across the growth curves of the mutants in our library to definitively identify any sporulation mutants based on growth alone (Fig. S4C). Germination dynamics after heat killing revealed that all strains were competent for

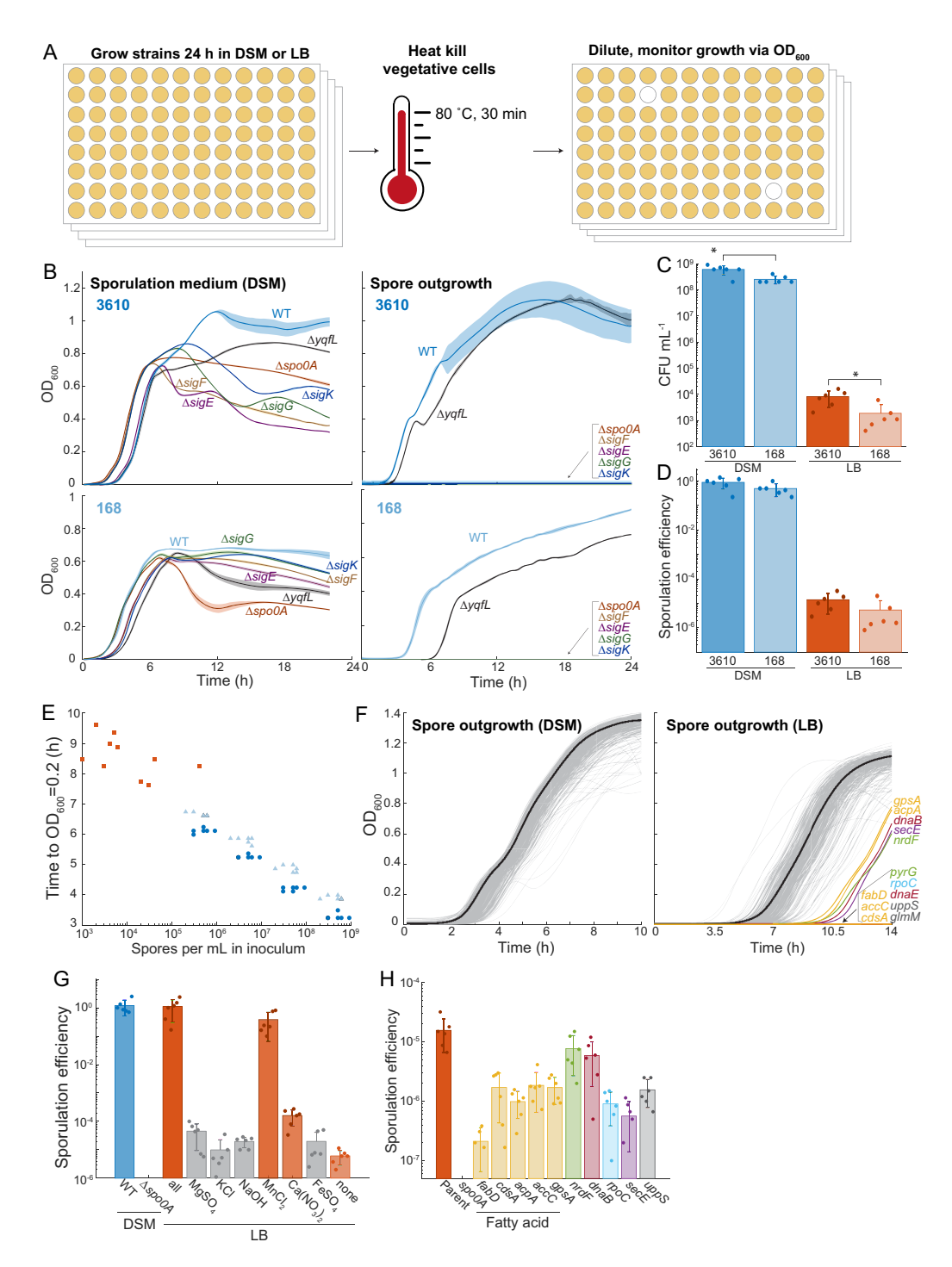


FIG 4 A high-throughput sporulation screen reveals reduced sporulation efficiency due to knockdown of fatty acid synthesis. (A) A growth-based, high-throughput assay was used to identify mutants defective in sporulation. Strains are grown to saturation, vegetative cells are heat killed, and cultures are inoculated into fresh medium. Any strains without viable spores will not survive the heat kill, and hence those wells will remain clear during outgrowth. (B) Sporulation mutants exhibit distinct patterns of growth in DSM (left) and are unable to outgrow after heat killing (right) for both strain 3610 (top) and strain 168 (bottom). Average growth curves over n=6 biological replicates are shown as solid lines, and shading represents 1 standard deviation. (C) There are fewer spores in a 24-h culture of strain 168 compared to strain 3610. Cultures were grown in DSM or LB, heat killed, and plated to measure CFU. *, P < 0.02. (D) The sporulation efficiency (ratio of CFU post- versus pre-heat killing) was lower for strain 168 than for strain 3610. (E) The number of spores in the inoculum correlates with growth lag. Cultures post-heat kill were serially diluted 10-fold, and growth curves were measured. The time to reach an OD₆₀₀ of 0.2 was negatively correlated with the number of spores (calculated from CFU). Dark blue circles represent strain 3610 grown in DSM, light blue triangles represent strain 168 grown in DSM, and orange squares represent strain 3610 grown in LB. (F) All essential gene basal knockdowns are

(Continued on next page)

sporulation and germination (Fig. 4F, left), indicating that basal expression levels of essential genes are sufficient for sporulation and germination after growth for 24 h in DSM.

Low sporulation efficiency in LB medium is enhanced through the addition of Mn²⁺ and Ca²⁺. Since all essential gene knockdown strains were capable of sporulation in DSM, we next focused on a medium in which *B. subtilis* shows reduced sporulation efficiency. Strain 3610 exhibited $\sim 100\%$ sporulation efficiency during growth in DSM. In contrast, in LB, the spore CFU per milliliter and sporulation efficiency of both 3610 and 168 were reduced 10^4 -fold (Fig. 4C and D).

Sporulation requires a combination of starvation and quorum sensing under specific conditions and is often assessed using the undefined medium DSM, which contains Difco nutrient broth and several additional components (Materials and Methods). Even though DSM promotes 10^4 -fold more sporulation than LB, growth of wild-type 3610 in DSM resulted in a similar yield to growth in LB (Fig. 4C and D; Fig. S4D). A previous study showed that Mn²+, one of the components of DSM, is critical for sporulation in DSM due, at least in part, to its effects on the enzyme phosphoglycerate phosphomutase (39). To further interrogate the differences in sporulation efficiency between DSM and LB, we investigated whether the supplements added to DSM affect sporulation in LB. Addition of all DSM supplements to LB raised sporulation efficiency to DSM levels, and MnCl₂ alone was sufficient to raise sporulation efficiency to near DSM levels (Fig. 4G). Furthermore, addition of Ca(NO₃)₂ to LB raised sporulation efficiency > 10-fold. The other supplements (MgSO₄, KCl, NaOH, and FeSO₄) did not significantly increase sporulation efficiency compared to unsupplemented LB (Fig. 4G). Thus, robust sporulation heavily depends on the addition of MnCl₂ and, to a lesser extent, Ca(NO₃)₂.

Lipid metabolism genes are involved in sporulation. Since culturing in LB medium resulted in vastly reduced sporulation (Fig. 4C and D), we screened our library in LB to identify gene knockdowns that impact sporulation. We identified several genes with reduced sporulation efficiency (Fig. 4F; Fig. S4E and Table S5). These hits were enriched for genes involved in lipid/fatty acid biosynthesis and metabolism (fabD, cdsA, acpA, accC, and gpsA; $P = 2.5 \times 10^{-3}$, DAVID enrichment score), as well as genes involved in cell wall synthesis (uppS and glmM), protein secretion (secE), transcription (rpoC), DNA replication (dnaB and dnaE), and nucleotide biosynthesis (nrdF and pyrG) (Fig. 4F; Table S5). Validation of these hits demonstrated that sporulation efficiency was reduced 10- to 100-fold in most cases (Fig. 4H). Intriguingly, despite exhibiting a delay in growth after heat killing (Fig. 4F; Fig. S4E), nrdF and dnaB had sporulation efficiencies that were only marginally lower than those of the parent, indicating that the delay may be due to slower germination rather than a reduction in spore number (Fig. 4H). Taken together, screening in a medium with generally lower sporulation efficiency revealed essential genes involved in sporulation and germination.

DISCUSSION

Here, we used a CRISPRi knockdown library to characterize phenotypes of each essential gene during liquid and colony growth. We found that gene essentiality was consistent between growth in liquid and on a surface as a colony. We also developed high-throughput screening platforms to quantify colony wrinkling and the degree of sporulation in liquid and discovered that fatty acid synthesis was a determinant of the degree of wrinkling and was important for proper sporulation. These findings extend our knowledge of the role played by essential genes during *B. subtilis* growth and development across lifestyles.

FIG 4 Legend (Continued)

competent for sporulation in DSM, and basal knockdown of fatty acid synthesis reduces sporulation in LB. The spore outgrowth curves following 24 h of growth in DSM (left) or LB (right) and heat killing are shown. Solid black lines show the average of parent controls (n=40 biological replicates), and light gray lines show growth curves of the CRISPRi library. For cultures pregrown in LB (right), several knockdowns exhibited a delay in growth or did not grow at all (colored lines). Fatty acid mutants are in yellow, DNA replication-related mutants are in red, ribosome-related mutants are in blue, cell-wall-related mutants are in gray, biosynthesis mutants are in green, and a secretion mutant is in purple. (G) Manganese and calcium nitrate promote sporulation in LB. The sporulation efficiency of strain 3610 (WT) in DSM and in LB with various DSM components added is shown. Note that the $\Delta spo0A$ mutant did not sporulate at all in DSM and hence is not plotted. Sporulation efficiencies in DSM and LB plus all additives were statistically indistinguishable (P=0.84). Sporulation efficiencies in LB+MnCl₂ and LB+Ca(NO₃)₂ were significantly higher than in LB without any additives (P<0.015). (H) Fatty acid knockdowns exhibit reduced sporulation efficiency in LB. Colors are the same as in panel F. The $\Delta spo0A$ mutant did not sporulate at all in LB and hence is not plotted. All knockdowns exhibited significantly different sporulation efficiency than the parent control (P<0.04).

Wrinkling is a hallmark property of *B. subtilis* pellicles and colony biofilms. Wrinkles require extracellular matrix, and they are able to transport liquid within the biofilm (15). Despite recognition that wrinkling is a complex feature of biofilms, it has been treated as a binary phenotype for the purpose of classifying mutants due to lack of methods for systematic quantification. Our image analysis platform enabled quantification of biofilm wrinkling, identifying that knockdown of gyrase or genes related to fatty acid synthesis increases wrinkling per unit area (Fig. 3C). Although wrinkling requires matrix expression and excess matrix can increase wrinkling (40), the knockdowns that we identified increased wrinkling in a manner uncorrelated with matrix expression (Fig. 3D). Thus, the mechanism or mechanisms by which reducing fatty acid synthesis or gyrase activity increases wrinkling remain mysterious and should be the subject of future study.

Sporulation is an important developmental process in a broad range of Gram-positive bacteria that has been extensively studied in B. subtilis laboratory strains. More than 150 nonessential genes have been linked to sporulation using screens that relied either on a change in the color of colonies of nonsporulating mutants or, more recently, on transposon sequencing (7). We found that sporulation mutants in strain 3610 remain opaque, motivating the design of a new sporulation screen based on growth following heat killing that provides a highly quantitative readout of sporulation efficiency (Fig. 4). Using this screen, all essential gene basal knockdowns were sporulation competent in the sporulation-inducing medium DSM (Fig. 4F); future CRISPRi systems that eliminate (or at least drastically reduce) the emergence of suppressors will enable the interrogation of sporulation during full knockdown of essential genes. In LB medium, sporulation efficiency was generally lower, and fatty acid mutants were among the knockdowns defective for sporulation (Fig. 4F). Notably, our screening strategy does not discriminate between sporulation and germination defects, and two mutants that exhibited near-wild-type sporulation efficiency were nevertheless identified by our screen (Fig. 4F and H), likely because they were delayed in germination, highlighting a strength of our assay. Unfortunately, the sporulation efficiency in LB is sufficiently low (\sim 1 spore in 10 5 cells) that a manual search for spores to track their germination dynamics is prohibitive without a way to enhance the fraction of spores in the starting culture. Such enrichment may be possible through fluorescence-activated cell sorter (FACS) sorting pre- or post-heat killing to isolate spore-sized cells for time-lapse imaging during germination. In addition to differences in colony coloration during sporulation between the lab strain 168 and the biofilm-forming strain 3610, strain 3610 also sporulated more readily in LB (Fig. 4C and D). Thus, although sporulation has been extensively studied in laboratory strains such as 168, the biofilm-forming strain 3610 and other environmental isolates may provide the key to further mechanistic insights into this process.

Given the observation that knockdown of fatty acid synthesis caused hyperwrinkled colonies (Fig. 3C) and reduced sporulation efficiency (Fig. 4F and H), future investigations should focus on whether the regulation of fatty acid synthesis mechanistically connects colony biofilm wrinkling and sporulation. Regardless, these findings add to a growing body of evidence linking fatty acid synthesis to a wide range of cellular processes in diverse bacteria, including *B. subtilis* sporulation (41–46). Fatty acid synthesis dictates cell size in *Escherichia coli* (47, 48), impacts biofilm formation in *Salmonella* (49), and is nonessential in some pathogens when host fatty acids are available (50). An improved understanding of the links between the biochemical effects of modulating fatty acid levels and other consequences such as changes to membrane potential may help to interpret our systems-level phenotypic quantifications. Together, our results demonstrate that CRISPRi essential gene knockdowns are an effective tool to uncover the role these genes play during biofilm and nonbiofilm growth and development of *B. subtilis*.

MATERIALS AND METHODS

Media. Strains were grown in LB (Lennox broth with 10 g/L tryptone, 5 g/L NaCl, and 5 g/L yeast extract) or MSgg medium (5 mM potassium phosphate buffer, diluted from 0.5 M stock with 2.72 g $\rm K_2HPO_4$ and 1.275 g $\rm KH_2PO_4$ and brought to pH 7.0 in 50 mL; 100 mM MOPS buffer [pH 7.0], adjusted with NaOH; 2 mM MgCl₂·6H₂O; 700 μ M CaCl₂·2H₂O; 100 μ M FeCl₃·6H₂O; 50 μ M MnCl₂·4H₂O; 1 μ M ZnCl₂; 2 μ M thiamine HCl; 0.5% [vol/vol] glycerol; and 0.5% [wt/vol] monosodium glutamate). MSgg medium was made fresh from stocks the day of each experiment for liquid cultures or a day before the experiment for agar plates. Glutamate and FeCl₃ stocks were made fresh weekly. Colonies were grown on 1.5% agar plates. TY medium was made for

phage transduction using the LB recipe described above supplemented with 10 mM MgSO₄ and 0.1 mM MnSO₄. DSM was made with 8 g/L Difco nutrient broth with 0.5 mL/L 1 M MgSO₄, 10 mL/L 10% (wt/vol) KCl, and 0.5 mL/L 1 M NaOH. After autoclaving and cooling, 1 mL/L 1 M Ca(NO₃)₂, 1 mL/L 0.1 M MnCl₂, and 1 mL/L 1 mM FeSO₄ were added. Xylose at a 1% (wt/vol) final concentration was used for full knockdowns. Antibiotics were used where indicated at the following concentrations: ampicillin (Amp), 100 μ g/mL; MLS (a combination of erythromycin and lincomycin) at 0.5 μ g/mL erythromycin and 12.5 μ g/mL lincomycin; chloramphenicol (Cm), 5 μ g/mL; tetracycline (Tet), 12.5 μ g/mL; and spectinomycin, (Spc), 100 μ g/mL.

Strain construction. All strains and their genotypes are listed in Table S1 in the supplemental material. The RFP depletion strain (HA13) was constructed using phage transduction (51), using HA12 as a parent and HA11 (CAG74226) as the donor. A 168 strain containing P_{xy7} dcas9 at the lacA locus (CAG74399) was used as a donor, and wild-type strain 3610 was used as the recipient to create the 3610-dCas9 parent strain (CAG74331/HA2) using MLS for selection.

For CRISPRi library construction, the 3610-dCas9 parent strain was used as the recipient and strains from a 168 CRISPRi library (16) were used as the donor. The phage transduction protocol was amended to increase the throughput of strain construction as follows. Donor strains were grown in 96-well deep-well plates (1-mL cultures in TY medium) for at least 5 h with shaking at 37°C and a Breathe-easy (Sigma-Aldrich) film covering the plate. A 0.1-mL sample of each of the 10^{-5} dilutions of fresh phage stocks grown on strain 3610 cells (10^{-5} was chosen as the dilution factor because it provided the appropriate level of lysis for our phage stock in a trial transduction) was aliquoted into 77 or 71 glass test tubes (each plate of the library contains 77 strains, except the fourth plate, which contains 71 strains). A 0.2-mL sample of each culture was added to the tubes, and the entire rack was incubated at 37°C for 15 min. Then, in batches of 11, 4 mL of TY molten soft agar (~55°C) were added to each phage-cell mixture, mixed gently, and poured onto TY plates so that the soft agar covered the entire plate. These plates were incubated at 37°C overnight in a single layer (not stacked). The next day, the plates were examined for lysis, 5 mL TY broth with 250 ng DNase was added to each plate, and the top agar was scraped with a 1-mL filter tip to liberate phage. The TY broth was then pipetted into a syringe attached to a 0.45-µm-pore filter and carefully filtered into a 5-mL conical vial. After being filtered, 1 mL of lysate was added to the appropriate well of a 96-well deepwell plate. Once all of the phage was isolated, we arrayed 10 μ L of each phage stock into 96-well microtiter plates. One hundred microliters of a saturated (>5 h of culturing, OD₆₀₀ of >1.5) culture was aliquoted into the wells containing phage and incubated for 25 min at 37°C without shaking. The phage-cell mixtures were plated onto selection plates (LB with chloramphenicol and 10 mM sodium citrate to select for the sgRNA locus), which were incubated for 18 h at 37°C. Any plates that did not have visible colonies after this incubation were incubated further at room temperature, and colonies generally appeared within a day. Transductant colonies were streaked for single colonies on LB+chloramphenicol plates, and a single colony for each strain in the library was stocked by growing in 5 mL LB on a roller drum at 37°C to mid- to late-log phase and then adding the culture to the appropriate well of a 96-well plate with a final concentration of 15% (vol/vol) glycerol. The library was stored at -80° C.

To generate mNeongreen reporter plasmid pKRH97, the promoter region of hag was PCR amplified from DK1042 chromosomal DNA using primers 5838 (5' AGGAGGGATCCTTATCGCGGAAAATAAACGAAGC 3')/5839 (5' CTCCTCTCGAGGAATATGTTGTTAAGGCACGTC 3') and digested with BamHI and XhoI. Next, the mNeongreen gene was PCR amplified from DK3394 using primers 5836 (5' AGGAGCTCGAGTAAGGAGGATTTTAGAATGGTTTCG AAAGGAGAGGAG 3')/5837 (5' CTCCTGAATTCTTACTTATAGAGTTCATCCATAC 3') and digested with Xhol and EcoRI. Both products were simultaneously ligated into the BamHI and EcoRI sites of pKM086 containing a polylinker and tetracycline resistance cassette between two arms of the ycqO gene (52). To generate the P_{exc} mNeongreen reporter plasmid pDP565, the promoter region of epsA (Pex) was PCR amplified from DK1042 chromosomal DNA using primers 7524 (5' AGGAGAAGCTTCCTGTCGTTATTTCGTTCATTA 3')/7525 (5' CTCCTCTCG AGCCCTTTCTGTTAATGATTGGATT 3'). The PCR product was digested with HindIII and XhoI and cloned into the HindIII and XhoI sites of plasmid pKRH97. To generate the P_{tapA} -mNeongreen reporter plasmid pDP575, the promoter region of tapA (PtapA) was PCR amplified from DK1042 chromosomal DNA using primers 7612 (5' AGGAGAAGCTTCCTTTTGGCTATAAGGATCAAATG 3')/7613 (5' CTCCTCTCGAGGTAAAACACTGTAACTTGATATG 3'). The PCR product was digested with HindIII and XhoI and cloned into the HindIII and XhoI sites of plasmid pKRH97. Strain DK1042 (53) was transformed with the above plasmids to integrate the constructs into the genome. The P_{ens} -mNeongreen construct was then transduced into DS6988, a $\Delta sinR \Delta eps$ recipient strain.

The amended phage transduction protocol above was used to make the CRISPRi candidate gene depletion reporter strains and the sporulation strains. Phage transduction was used to introduce the P_{epsA} (HA1463 donor) and P_{tapA} (HA1502 donor) reporter constructs into parent strain HA2 containing $P_{xyr}dcas9$ to create parent strains HA1464 (parent P_{eps}) and HA1505 (parent P_{tapA}). These parents were used as recipient strains and the strain 168 CRISPRi strains as donors for phage transduction (16). HA395 and HA396 were used as parents to introduce the reporter constructs into $\Delta sinI$ and $\Delta sinR$ strains, respectively. For sporulation strains, we used strain 3610 (HA10) as the recipient and strains HA1163 to HA1172 as donors for phage transduction (Table S1).

CRISPRi targeting of RFP in colonies and biofilms. Wild-type 3610, parent-RFP, and CRISPRi-RFP strains were cultured in 5-mL test tubes at 37°C to an OD $_{600}$ of \sim 1 in liquid LB. The parent-RFP strain was spotted onto LB and MSgg agar plates without xylose, while the CRISPRi-RFP strain was spotted onto LB and MSgg agar in 12-well plates containing 0.0005% to 1% (wt/vol) xylose. Each well of the plate had \sim 1 mL medium to maintain the proper focal plane. Colonies were incubated at 30°C for 48 h inside a box in a warm room to prevent the plates from drying out. RFP fluorescence of the colonies was imaged with a Typhoon FLA 9500 scanner using the multiplate drawer, with plates inserted face up so the scanner imaged through the agar. RFP signal was acquired with a 532-nm laser and a long-pass green filter. FIJI was used to quantify the fluorescence intensity of each colony: the images were first inverted so the background was black and RFP signal was white, and fluorescence of each colony was measured using a circle the size of the largest colony. The wild-type 3610 measurement was subtracted as a blank, and values were normalized to the 100% RFP colony.

Liquid growth assays for the CRISPRi library. Freezer stocks were pinned onto agar plates using sterile 96 long-pin Singer RePads (REP-001) and grown overnight at 37°C to form colonies. Sterile 96 long-pin Singer RePads were used to manually inoculate the colonies into 200 μ L of LB in a 96-well microtiter plate. Parent controls were added to empty wells on each plate. The plate was sealed with optical film, and a syringe needle was used to poke off-center holes above each well to allow air exchange in the headspace and grown with linear shaking at 37°C for \sim 5 h until the parent control reached an OD₆₀₀ of \sim 1. The plate was diluted 1:200 into 200 μ L of the appropriate medium, and growth was monitored on a Biotek Epoch plate reader at 30°C with linear shaking (567 cycles/min, 3-mm magnitude). The minimum value of a blank well was used as the blank.

Liquid growth assays for follow-up experiments. Strains were streaked out for individual colonies from glycerol stocks onto LB agar plates and incubated at 37°C overnight. Single colonies were outgrown in 200 μ L of LB in a 96-well microtiter plate at 37°C for \sim 5 h until WT/parent strains reached an OD₆₀₀ of \sim 1. Cultures were diluted 1:200 into 200 μ L of the appropriate medium, the plate was sealed with an optical seal with holes poked off-center for air exchange, and growth was monitored using a Biotech Epoch plate reader at 30°C (asnB knockdown) or 37°C (mapA, glyA, and folD knockdowns) with linear shaking (567 cycles/min, 3-mm magnitude). Before inoculation, the medium-containing microtiter plates were preblanked to enable accurate measurements of growth (54).

Growth assay of colonies on agar plates. Freezer stocks were pinned onto agar plates using sterile 96 long-pin Singer RePads and grown overnight at 37°C to form colonies. Sterile 96 long-pin Singer RePads were used to inoculate the colonies into 200 μ L of LB in a 96-well microtiter plate. Parent controls were added to empty wells on each plate. The plate was sealed with an optical seal with holes poked off-center for air exchange and grown with linear shaking at 37°C for \sim 5 h until the parent control reached an OD₆₀₀ of \sim 1. Approximately 1 μ L was spotted onto an agar plate (poured the day before, dried at room temperature overnight, and then dried at 37°C for 1 h before spotting) using a Singer robot (spotting was repeated 12 times with a Singer RePad), and colonies were grown at 30°C in a single layer inside a box or plastic bag to prevent the plates from drying out. Images were taken 24 h postspotting for colony size analyses and 48 h postspotting for biofilm wrinkling analyses. For follow-up assays of candidate gene knockdown strains, the same protocol was used, except that freezer stocks were streaked out for individual colonies that were used for inoculation.

Colony imaging. Images were acquired with a Canon EOS Rebel T5i EF-S with a Canon Ef-S 60-mm f/2.8 Macro USM fixed lens. The digital single-lens reflex (DSLR) camera was set up at a fixed height in a light box. Lighting and camera settings were maintained for the duration of the experiment, using the "manual" mode on the camera. The EOS Utility software was used to run the camera. Plates were imaged colony side up to avoid imaging through the agar.

Colony size analysis. Colony size was measured in FIJI by diagonally bisecting the center of the colony. Colony size was assayed based on images acquired at 24 h, which was before the colonies were noticeably affected by the growth of neighbors or the edge of the plate.

Wrinkling quantification. Images were analyzed with custom Matlab code (https://doi.org/10.25740/nt084hv1801). In brief, images were rotated so that the boundaries of the plate were aligned with the horizontal and vertical axes. Images were converted to grayscale. To account for uneven lighting across the image, the background intensity profile was computed using a disk-shaped structured element of size 15 pixels and was subtracted from the image. Background-subtracted images were contrast adjusted and converted to a binarized image using the Matlab function im2bw with default parameters. These binarized images were typically a reasonable proxy for the positions of wrinkles. All connected components with fewer than 50 pixels were removed using the Matlab function bwareaopen. The center of one of the corner colonies was manually recorded using the Matlab function ginput, and the centers of the other colonies were inferred based on the known grid spacing. The wrinkling intensity was computed as a function of radial distance *r* by summing the pixels within a circle of radius *r*. The value used to calculate the reported wrinkling density was the radius of the colony as measured in FIJI, and the total intensity was normalized to colony area. Note that the *sufD* strain was misclassified due to a lighting artifact (Fig. S3A).

mNeongreen reporter assay. Strains from glycerol stocks were streaked out for single colonies, and plates were incubated at 37°C overnight. Individual colonies were picked into 200 μ L of LB medium in a 96-well plate and grown at 37°C with linear shaking until the parent/wild-type controls reached an OD₆₀₀ of \sim 1. One microliter of culture was spotted onto MSgg agar rectangular plates (poured the day before, dried overnight at room temperature and 1 h at 37°C before spotting; \sim 30 mL of medium was used). Plates were incubated in a box at 30°C for 16 h. Plates were imaged with a Typhoon FLA 9500 scanner using the multiplate drawer, inserted face up so that the scanner imaged through the agar. mNeongreen signal was acquired with a 473-nm laser and a long-pass blue filter. Images were inverted so the background was dark and fluorescence was in white, and fluorescence intensity was measured in FIJI using a circle the size of the largest colony. Colony size was measured diagonally with a line bisecting the center of the colony to calculate intensity per unit area.

Essential gene bioinformatic comparison. A bash script was used to compare the protein sequences of essential genes in strain 168 (PRJNA57675_168.fasta) with their homologs in strain 3610 (PRJNA377766_3610.fasta), and any mismatches were identified using custom Matlab code. Any genes with potential protein coding differences between strains 168 and 3610 were tested using BLAST (https://blast.ncbi.nlm.nih.gov) with the NCBI strain 3610 genome from GenBank (accession no. CP034484.1) and the strain 168 genome from SubtiWiki (55).

Sporulation assay. The library was grown from colonies at 37°C for ~ 5 h so that the wild-type strain reached an OD_{600} of ~ 1 in a plate reader with linear shaking. Cultures were diluted 1:200 either using a Singer robot (for DSM experiments) or by manual pipetting (for LB experiments) and grown for 24 h at 37°C in a Biotek Epoch plate reader with linear shaking (567 cycles/min, 3-mm magnitude). At 24 h, vegetative cells were heat killed by transferring the sealed plates to an oven at 80°C for 30 min with preheated heat blocks

placed on top of the plates to prevent condensation on the seal. Seals were carefully removed post-heat kill, and cultures were diluted 1:200 into LB. To monitor germination, cultures were grown at 37°C in an Epoch plate reader with linear shaking for 24 h. Plates were preblanked before inoculation to enable accurate measurements of growth (54). For follow-up assays to confirm delayed growth phenotypes, strains were streaked out for individual colonies, plates were incubated overnight at 37°C, and individual colonies were inoculated into each well of a 96-well plate for outgrowth following the sporulation assay as described above.

Sporulation and plating efficiency. Cultures were grown as above in the sporulation efficiency assay. Serial dilutions of cultures before and after heat killing were plated to quantify total viable cells and surviving spores, respectively. Seals were removed to perform the serial dilution, then plates were resealed with a new seal before heat killing. Cultures were diluted with 10 μ L into 90 μ L in V-bottom plates and pipetted up and down several times to mix using new pipette tips for each dilution. Ten microliters of each dilution were spotted using a BenchSmart (Rainin) liquid handling robot. Plates were incubated overnight at 37°C, and colonies were counted. For the spore dilution experiment, the plating efficiency of undiluted heat-killed spores was measured as described above. Tenfold serial dilutions of the heat-killed culture were then used to inoculate LB (1 μ L into 200 μ L), and growth was monitored as described above.

Determining genes required for growth in liquid and agar. Twelve strains were unable to grow under full induction in liquid despite being able to grow as a colony on LB+xylose and MSgg+xylose. However, these gene knockdowns exhibited 10^3 - to 10^4 -fold reductions in plating efficiency (determined as described above with serial dilutions and plating) relative to the parent strain (Fig. S2D and E), consistent with their growth defects in liquid. Thus, these 12 strains were presumed to be incorrectly classified based on our colony screen.

Data availability. All scripts used for comparison of protein sequences are available in the Stanford Digital Repository at https://purl.stanford.edu/fb108cz5121. All Matlab code used for quantifying wrinkling are available at https://purl.stanford.edu/nt084hv1801.

SUPPLEMENTAL MATERIAL

Supplemental material is available online only.

FIG S1, PDF file, 0.7 MB.

FIG S2, PDF file, 0.4 MB.

FIG S3, PDF file, 0.9 MB.

FIG S4, PDF file, 0.8 MB.

TABLE \$1, XLSX file, 0.02 MB.

TABLE S2, XLSX file, 0.01 MB.

TABLE S3, XLSX file, 0.01 MB.

TABLE S4, XLSX file, 0.01 MB.

TABLE S5, XLSX file, 0.01 MB.

TABLE S6, XLSX file, 0.01 MB.

ACKNOWLEDGMENTS

We thank the Huang lab and Zachary Hallberg for helpful discussions.

We acknowledge support from the Allen Discovery Center at Stanford on Systems Modeling of Infection (to H.A.A. and K.C.H.), NIH R35 GM118061 (to C.G.), NIH RM1 Award GM135102 (to K.C.H.), and NSF Awards EF-2125383 and IOS-2032985 (to K.C.H.). K.C.H. is a Chan Zuckerberg Biohub Investigator.

REFERENCES

- 1. Lopez D, Vlamakis H, Kolter R. 2010. Biofilms. Cold Spring Harb Perspect Biol 2:a000398. https://doi.org/10.1101/cshperspect.a000398.
- Aguilar C, Vlamakis H, Losick R, Kolter R. 2007. Thinking about *Bacillus subtilis* as a multicellular organism. Curr Opin Microbiol 10:638–643. https://doi.org/ 10.1016/j.mib.2007.09.006.
- Lyons NA, Kolter R. 2015. On the evolution of bacterial multicellularity. Curr Opin Microbiol 24:21–28. https://doi.org/10.1016/j.mib.2014.12.007.
- 4. Arnaouteli S, Bamford NC, Stanley-Wall NR, Kovacs AT. 2021. *Bacillus subtilis* biofilm formation and social interactions. Nat Rev Microbiol 19: 600–614. https://doi.org/10.1038/s41579-021-00540-9.
- Tan IS, Ramamurthi KS. 2014. Spore formation in *Bacillus subtilis*. Environ Microbiol Rep 6:212–225. https://doi.org/10.1111/1758-2229.12130.
- Koo BM, Kritikos G, Farelli JD, Todor H, Tong K, Kimsey H, Wapinski I, Galardini M, Cabal A, Peters JM, Hachmann AB, Rudner DZ, Allen KN, Typas A, Gross CA. 2017. Construction and analysis of two genome-scale deletion libraries for *Bacillus subtilis*. Cell Syst 4:291–305.e7. https://doi .org/10.1016/j.cels.2016.12.013.
- Meeske AJ, Rodrigues CD, Brady J, Lim HC, Bernhardt TG, Rudner DZ. 2016.
 High-throughput genetic screens identify a large and diverse collection of

- new sporulation genes in *Bacillus subtilis*. PLoS Biol 14:e1002341. https://doi.org/10.1371/journal.pbio.1002341.
- Dragos A, Kiesewalter H, Martin M, Hsu CY, Hartmann R, Wechsler T, Eriksen C, Brix S, Drescher K, Stanley-Wall N, Kummerli R, Kovacs AT. 2018. Division of labor during biofilm matrix production. Curr Biol 28:1903–1913.e5. https://doi. org/10.1016/j.cub.2018.04.046.
- 9. Vlamakis H, Chai Y, Beauregard P, Losick R, Kolter R. 2013. Sticking together: building a biofilm the *Bacillus subtilis* way. Nat Rev Microbiol 11: 157–168. https://doi.org/10.1038/nrmicro2960.
- Sanchez-Vizuete P, Dergham Y, Bridier A, Deschamps J, Dervyn E, Hamze K, Aymerich S, Le Coq D, Briandet R. 2022. The coordinated population redistribution between *Bacillus subtilis* submerged biofilm and liquid-air pellicle. Biofilm 4:100065. https://doi.org/10.1016/j.biofilm.2021.100065.
- Porter M, Davidson FA, MacPhee C, Stanley-Wall N. 2022. Systematic microscopical analysis reveals obligate synergy between extracellular matrix components during *Bacillus subtilis* colony biofilm development. bioRxiv. https://www.biorxiv.org/content/10.1101/2022.06.16.496330v1.
- Asally M, Kittisopikul M, Rué P, Du Y, Hu Z, Çağatay T, Robinson AB, Lu H, Garcia-Ojalvo J, Süel GM. 2012. Localized cell death focuses mechanical

- forces during 3D patterning in a biofilm. Proc Natl Acad Sci U S A 109: 18891–18896. https://doi.org/10.1073/pnas.1212429109.
- Trejo M, Douarche C, Bailleux V, Poulard C, Mariot S, Regeard C, Raspaud E. 2013. Elasticity and wrinkled morphology of *Bacillus subtilis* pellicles. Proc Natl Acad Sci U S A 110:2011–2016. https://doi.org/10.1073/pnas.1217178110.
- Schultz D, Onuchic JN, Ben-Jacob E. 2012. Turning death into creative force during biofilm engineering. Proc Natl Acad Sci U S A 109:18633–18634. https://doi.org/10.1073/pnas.1215227109.
- Wilking JN, Zaburdaev V, De Volder M, Losick R, Brenner MP, Weitz DA. 2013. Liquid transport facilitated by channels in *Bacillus subtilis* biofilms. Proc Natl Acad Sci U S A 110:848–852. https://doi.org/10.1073/pnas.1216376110.
- Peters JM, Colavin A, Shi H, Czarny TL, Larson MH, Wong S, Hawkins JS, Lu CHS, Koo BM, Marta E, Shiver AL, Whitehead EH, Weissman JS, Brown ED, Qi LS, Huang KC, Gross CA. 2016. A comprehensive, CRISPR-based functional analysis of essential genes in bacteria. Cell 165:1493–1506. https:// doi.org/10.1016/j.cell.2016.05.003.
- Arjes HA, Willis L, Gui H, Xiao Y, Peters J, Gross C, Huang KC. 2021. Threedimensional biofilm colony growth supports a mutualism involving matrix and nutrient sharing. eLife 10:e64145. https://doi.org/10.7554/eLife.64145.
- McLoon AL, Guttenplan SB, Kearns DB, Kolter R, Losick R. 2011. Tracing the domestication of a biofilm-forming bacterium. J Bacteriol 193:2027–2034. https://doi.org/10.1128/JB.01542-10.
- Todter D, Gunka K, Stulke J. 2017. The highly conserved Asp23 family protein YqhY plays a role in lipid biosynthesis in *Bacillus subtilis*. Front Microbiol 8:883. https://doi.org/10.3389/fmicb.2017.00883.
- McKie SJ, Neuman KC, Maxwell A. 2021. DNA topoisomerases: advances in understanding of cellular roles and multi-protein complexes via structure-function analysis. Bioessays 43:e2000286. https://doi.org/10.1002/bies.202000286.
- Orr E, Staudenbauer WL. 1982. Bacillus subtilis DNA gyrase: purification of subunits and reconstitution of supercoiling activity. J Bacteriol 151:524–527. https://doi.org/10.1128/jb.151.1.524-527.1982.
- Samadpour AN, Merrikh H. 2018. DNA gyrase activity regulates DnaA-dependent replication initiation in *Bacillus subtilis*. Mol Microbiol 108: 115–127. https://doi.org/10.1111/mmi.13920.
- Oknin H, Steinberg D, Shemesh M. 2015. Magnesium ions mitigate biofilm formation of *Bacillus* species via downregulation of matrix genes expression. Front Microbiol 6:907. https://doi.org/10.3389/fmicb.2015.00907.
- 24. Youngman P, Zuber P, Perkins JB, Sandman K, Igo M, Losick R. 1985. New ways to study developmental genes in spore-forming bacteria. Science 228:285–291. https://doi.org/10.1126/science.228.4697.285.
- 25. Takahashi I. 1965. Transduction of sporogenesis in *Bacillus subtilis*. J Bacteriol 89:294–298. https://doi.org/10.1128/jb.89.2.294-298.1965.
- Sandman K, Losick R, Youngman P. 1987. Genetic analysis of *Bacillus subtilis spo* mutations generated by Tn917-mediated insertional mutagenesis. Genetics 117:603–617. https://doi.org/10.1093/genetics/117.4.603.
- 27. Rogolsky M. 1968. Genetic mapping of a locus which regulates the production of pigment associated with spores of *Bacillus subtilis*. J Bacteriol 95:2426–2427. https://doi.org/10.1128/jb.95.6.2426-2427.1968.
- Freese E, Fortnagel P. 1967. Analysis of sporulation mutants. I. Response of uracil incorporation to carbon sources, and other mutant properties. J Bacteriol 94:1957–1969. https://doi.org/10.1128/jb.94.6.1957-1969.1967.
- Coote JG. 1972. Sporulation in *Bacillus subtilis*. Characterization of oligosporogenous mutants and comparison of their phenotypes with those of asporogenous mutants. J Gen Microbiol 71:1–15. https://doi.org/10.1099/00221287-71-1-1.
- Molle V, Fujita M, Jensen ST, Eichenberger P, Gonzalez-Pastor JE, Liu JS, Losick R. 2003. The Spo0A regulon of *Bacillus subtilis*. Mol Microbiol 50: 1683–1701. https://doi.org/10.1046/j.1365-2958.2003.03818.x.
- 31. Fujita M, Gonzalez-Pastor JE, Losick R. 2005. High- and low-threshold genes in the Spo0A regulon of *Bacillus subtilis*. J Bacteriol 187:1357–1368. https://doi.org/10.1128/JB.187.4.1357-1368.2005.
- 32. Britton RA, Eichenberger P, Gonzalez-Pastor JE, Fawcett P, Monson R, Losick R, Grossman AD. 2002. Genome-wide analysis of the stationary-phase sigma factor (sigma-H) regulon of Bacillus subtilis. J Bacteriol 184: 4881–4890. https://doi.org/10.1128/JB.184.17.4881-4890.2002.
- Eichenberger P, Fujita M, Jensen ST, Conlon EM, Rudner DZ, Wang ST, Ferguson C, Haga K, Sato T, Liu JS, Losick R. 2004. The program of gene transcription for a single differentiating cell type during sporulation in *Bacillus subtilis*. PLoS Biol 2:e328. https://doi.org/10.1371/journal.pbio.0020328.
- 34. Eichenberger P, Jensen ST, Conlon EM, van Ooij C, Silvaggi J, Gonzalez-Pastor JE, Fujita M, Ben-Yehuda S, Stragier P, Liu JS, Losick R. 2003. The *sigmaE*

- regulon and the identification of additional sporulation genes in *Bacillus subtilis*. J Mol Biol 327:945–972. https://doi.org/10.1016/s0022-2836(03)00205-5.
- Silvaggi JM, Popham DL, Driks A, Eichenberger P, Losick R. 2004. Unmasking novel sporulation genes in *Bacillus subtilis*. J Bacteriol 186:8089–8095. https://doi.org/10.1128/JB.186.23.8089-8095.2004.
- Wang ST, Setlow B, Conlon EM, Lyon JL, Imamura D, Sato T, Setlow P, Losick R, Eichenberger P. 2006. The forespore line of gene expression in *Bacillus subtilis*. J Mol Biol 358:16–37. https://doi.org/10.1016/j.jmb.2006.01.059.
- Donovan W, Zheng LB, Sandman K, Losick R. 1987. Genes encoding spore coat polypeptides from *Bacillus subtilis*. J Mol Biol 196:1–10. https://doi.org/10.1016/0022-2836(87)90506-7.
- Arjes HA, Vo L, Dunn CM, Willis L, DeRosa CA, Fraser CL, Kearns DB, Huang KC. 2020. Biosurfactant-mediated membrane depolarization maintains viability during oxygen depletion in *Bacillus subtilis*. Curr Biol 30:1011–1022.e6. https://doi.org/10.1016/j.cub.2020.01.073.
- Vasantha N, Freese E. 1979. The role of manganese in growth and sporulation of *Bacillus subtilis*. J Gen Microbiol 112:329–336. https://doi.org/10.1099/ 00221287-112-2-329.
- Limoli DH, Jones CJ, Wozniak DJ. 2015. Bacterial extracellular polysaccharides in biofilm formation and function. Microbiol Spectr 3:10.1128/microbiolspec.MB-0011-2014. https://doi.org/10.1128/microbiolspec.MB-0011-2014.
- 41. Haggett L, Bhasin A, Srivastava P, Fujita M. 2018. A revised model for the control of fatty acid synthesis by master regulator Spo0A in *Bacillus subtilis*. Mol Microbiol 108:424–442. https://doi.org/10.1111/mmi.13945.
- 42. Narula J, Fujita M, Igoshin OA. 2016. Functional requirements of cellular differentiation: lessons from *Bacillus subtilis*. Curr Opin Microbiol 34: 38–46. https://doi.org/10.1016/j.mib.2016.07.011.
- Narula J, Kuchina A, Zhang F, Fujita M, Suel GM, Igoshin OA. 2016. Slow-down of growth controls cellular differentiation. Mol Syst Biol 12:871. https://doi.org/10.15252/msb.20156691.
- Pedrido ME, de Ona P, Ramirez W, Lenini C, Goni A, Grau R. 2013. Spo0A links de novo fatty acid synthesis to sporulation and biofilm development in *Bacillus* subtilis. Mol Microbiol 87:348–367. https://doi.org/10.1111/mmi.12102.
- Perez CA, Marini P, de Mendoza D. 1998. Effects on *Bacillus subtilis* of conditional expression of the *accBC* operon encoding subunits of acetyl coenzyme A carboxylase, the first enzyme of fatty acid synthesis. Microbiology (Reading) 144:895–903. https://doi.org/10.1099/00221287-144-4-895.
- 46. Schujman GE, Grau R, Gramajo HC, Ornella L, de Mendoza D. 1998. *De novo* fatty acid synthesis is required for establishment of cell type-specific gene transcription during sporulation in *Bacillus subtilis*. Mol Microbiol 29:1215–1224. https://doi.org/10.1046/j.1365-2958.1998.01004.x.
- Vadia S, Tse JL, Lucena R, Yang Z, Kellogg DR, Wang JD, Levin PA. 2017. Fatty acid availability sets cell envelope capacity and dictates microbial cell size. Curr Biol 27:1757–1767.e5. https://doi.org/10.1016/j.cub.2017.05.076.
- Yao Z, Davis RM, Kishony R, Kahne D, Ruiz N. 2012. Regulation of cell size in response to nutrient availability by fatty acid biosynthesis in *Escherichia coli*. Proc Natl Acad Sci U S A 109:E2561–E2568. https://doi.org/10.1073/pnas.1209742109.
- Hermans K, Roberfroid S, Thijs IM, Kint G, De Coster D, Marchal K, Vanderleyden J, De Keersmaecker SC, Steenackers HP. 2016. FabR regulates *Salmonella* biofilm formation via its direct target FabB. BMC Genomics 17:253. https://doi.org/10 .1186/s12864-016-2387-x.
- Brinster S, Lamberet G, Staels B, Trieu-Cuot P, Gruss A, Poyart C. 2009.
 Type II fatty acid synthesis is not a suitable antibiotic target for Gram-positive pathogens. Nature 458:83–86. https://doi.org/10.1038/nature07772.
- Yasbin RE, Young FE. 1974. Transduction in *Bacillus subtilis* by bacteriophage SPP1. J Virol 14:1343–1348. https://doi.org/10.1128/JVI.14.6.1343-1348.1974.
- Mohamed AMT, Chan H, Luhur J, Bauda E, Gallet B, Morlot C, Cole L, Awad M, Crawford S, Lyras D, Rudner DZ, Rodrigues CDA. 2021. Chromosome segregation and peptidoglycan remodeling are coordinated at a highly stabilized septal pore to maintain bacterial spore development. Dev Cell 56:36–51.e5. https://doi.org/10.1016/j.devcel.2020.12.006.
- Konkol MA, Blair KM, Kearns DB. 2013. Plasmid-encoded Coml inhibits competence in the ancestral 3610 strain of *Bacillus subtilis*. J Bacteriol 195:4085–4093. https://doi.org/10.1128/JB.00696-13.
- 54. Atolia E, Cesar S, Arjes HA, Rajendram M, Shi H, Knapp BD, Khare S, Aranda-Diaz A, Lenski RE, Huang KC. 2020. Environmental and physiological factors affecting high-throughput measurements of bacterial growth. mBio 11:e01378-20. https://doi.org/10.1128/mBio.01378-20.
- Pedreira T, Elfmann C, Stulke J. 2022. The current state of SubtiWiki, the database for the model organism *Bacillus subtilis*. Nucleic Acids Res 50: D875–D882. https://doi.org/10.1093/nar/gkab943.